Simultaneous measurement of single cell mechanics and cell-to-materials adhesion using fluidic force microscopy

Ma Luo[†], Wenjian Yang[†,#], Tyrell N. Cartwright[‡], Jonathan M.G. Higgins[‡], and Jinju Chen[†]*

[†] School of Engineering, Newcastle University, Newcastle Upon Tyne, NE1 7RU, UK; [#] Research Center for Intelligent Sensing Systems, Zhijiang Laboratory, Hangzhou, 311100, China; [‡] Biosciences Institute, Faculty of Medical Sciences, Newcastle University, Framlington Place, Newcastle upon Tyne, NE2 4HH, UK.

* Correspondence and requests for materials should be addressed to J.C. (email: jinju.chen@ncl.ac.uk)

ABSTRACT

The connection between cells and their substrate is essential for biological processes such as cell migration. Atomic force microscopy nanoindentation has often been adopted to measure single cell mechanics. Very recently, fluidic force microscopy has been developed to enable rapid measurements of cell adhesion. However, simultaneous characterization of the cell-to-material adhesion and viscoelastic properties of the same cell is challenging. In this study, we present a new approach to simultaneously determine these properties for single cells, using fluidic force microscopy. For MCF-7 cells grown on tissue-culture-treated polystyrene surfaces, we found that the adhesive force and adhesion energy were correlated for each cell. Well-spread cells tended to have stronger adhesion, which may be due to the greater area of the contact between cellular adhesion receptors and the surface. By contrast, the viscoelastic properties of MCF-7 cells cultured on the same surface appeared to have little dependence on cell shape. This methodology provides an integrated approach to better understand the biophysics of multiple cell types.

INTRODUCTION

Cell mechanics of living cells are vital for many cell functions, including mechanotransduction[1-3], migration, and differentiation[4]. It is known that changes in cell mechanics are often correlated with disease progression[5-12]. Cell-matrix adhesion is important for the patterning, integrity and homeostasis of tissues, and may provide a target for therapy, for example in cancer metastasis [13]. Cell mechanics and the adhesion between cells and matrix are also important for tissue engineering. Therefore, it is important to study cell mechanics and cell-to-material adhesion.

Atomic Force Microscope (AFM) has been widely adopted for mechanical characterization of multiple cell types (for example cancerous cells)[14], including elastic moduli and viscoelastic moduli. AFM with spherical probes has been widely adopted to measure the mechanical properties of the whole cell[14-17] while, for the determination of spatial dependent mechanical properties across the cell, pyramid probes have been preferred [18-21]. No matter which probe is used, it is essential to adopt appropriate mechanical models with regard to the testing protocols[14]. Otherwise, it may lead to significant errors in determining the mechanical properties of cells[15, 22, 23]. These errors are often caused by ignoring the loading effect on the apparent modulus. In which case, a mathematical model is required to take this into account. Additionally, these analytical models also need to be modified to include the large deformation effect[15, 23, 24].

In addition, tipless AFM cantilevers have been adopted to measure the adhesion between cells and substrates. This approach requires functionalization of the cantilever to facilitate strong adhesion to the cell of interest[25-27]. However, this method is tedious and time-consuming. Furthermore, it is difficult to guarantee that cell-cantilever adhesion is stronger than cell-substrate adhesion. For example, during the detachment tests, cells may detach from the cantilever as often as from the substrate[28].

More recently, a new technique, fluidic force microscopy (FluidFM) has been developed that enables rapid attachment of a probe to cells, in combination with the accurate force-controlled positioning of AFM [29-34]. In this case, a microsized channel is integrated in an AFM cantilever and connected via channels in the AFM chip holder, thus creating a continuous and closed fluidic channel that can be filled with fluid such as deionized water. An aperture in the AFM tip at the end of the cantilever allows liquids to be dispensed locally. Negative pressure can be applied to the cell to attach it to the cantilever, and retraction of the cantilever can then detach the cell from the surface (Figure 1). Force feedback is ensured by a standard AFM laser detection system that measures the deflection of the cantilever and the force applied by the tip to the sample during the process of approach and detachment. Force-displacement curves can be recorded during detachment, and thus the adhesive force and adhesion energy can be determined. This technique is particularly useful to measure strong adhesion between cells and materials[34].

The cytoskeleton is the main source of cell stiffness, and its elasticity can resist the deformation forces caused by extracellular mechanical events impinging upon cells. Force on the cell membrane is sensed by the cytoskeleton, and can upregulate the formation of focal adhesions, altering cell-to-matrix adhesion [35, 36]. Measuring the adhesion and stiffness of the same cell allows characterization of this mechanotransduction mechanism. The viscoelastic cell deformation is often intertwined with cell adhesion during the detachment process of cells. Both viscoelastic properties and cell-to-material adhesion play roles in determining how cells migrate in response to the mechanical stimuli. The capacity to simultaneously determine the

viscoelastic properties and adhesion of a single cell can facilitate an understanding of the correlation between them, and how they collectively affect cell migration. However, this has not been achieved previously because the tipless-cantilever-based technique focuses only on pulling the cell away from the surface, and the cell deformation cannot be monitored. Furthermore, the tipless cantilever requires sufficiently long contact time between the functionalized cantilever and the cell to form a strong bond, which might affect the cell mechanics because the cell is now bonded to two solid surfaces.

Although a recent study used FluidFM in an effort to simultaneously determine the viscoelastic and adhesion properties of a single cell, its method to extract and analysis elastic moduli was merely based on the analysis of detachment curve. It was assumed that the slope of the detachment curve was cell stiffness [37]. Indeed, it may be relevant to cell stiffness but mainly reflects interfacial properties [38].

In this work, we used FluidFM to simultaneously measure cell viscoelasticity and cell-to-surface adhesion forces, and to enable us to understand mechanics of cell heterogeneity. We utilised MCF-7 cells because they are well-studied human breast cancer cells with abundant biophysical data available for comparison. A better understanding of the mechanical properties of breast cancer cells is likely also to contribute to the design of improved treatments for breast cancer, which has the second highest incidence of all cancers in women worldwide and is the fourth most common cause of cancer mortality[39]. The technique developed here could also be adopted to measure the mechanical properties and adhesion for core/shell particles for use in semiconductors[40], catalysts[41], solar cells[42], drug delivery[43] and biotechnology[44] as well as typical biomaterials like cellulose[45].

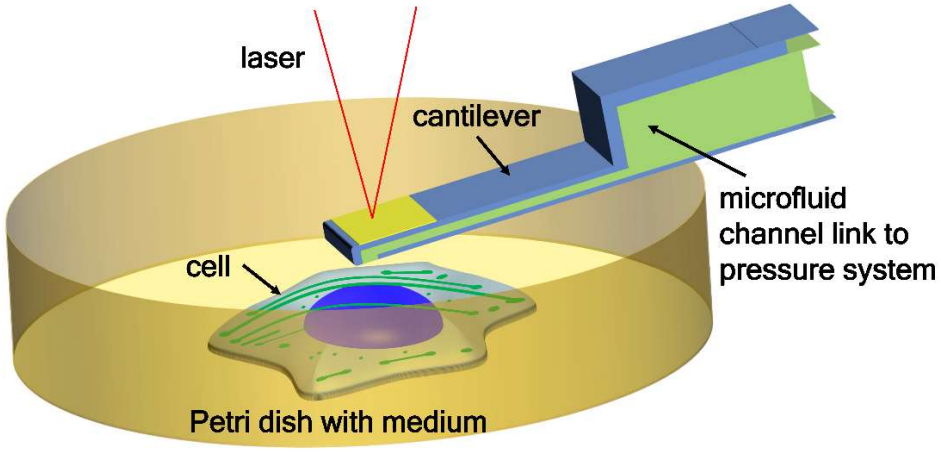

Figure 1. Schematic diagram of FluidFM for cell mechanics and cell adhesion measurements. During liquid dispensing, the cell and substrate can be simultaneously observed with an optical microscope, either through the transparent probe holder or the low clearance petri dish.

MATERIALS AND METHODS

Cell culture: MCF-7 cells were cultured in DMEM (Dulbecco's Modified Eagle Medium, Sigma Aldrich) with 10% FBS (Fetal Bovine Serum, Sigma Aldrich) and 1% Penicillin-Streptomycin (Thermo Fisher Scientific) in T75 flasks (Thermo Fisher Scientific) at 37°C, 5% CO_2 in a 95% relative humidity incubator. Cells were split when they grew to 80% confluence. For confocal microscopy, nanoindentation and adhesion experiments, cells were seeded and cultured in tissue culture treated polystyrene petri dishes (μ-Dish, 50 mm with ibiTreat surface, Ibidi) for 1 day at 37°C, 5% CO_2 95% relative humidity. These dishes enabled cell adherence and proliferation on the surface without additional surface coatings. They also have low clearance required for FluidFM.

Confocal imaging

To determine surface contact areas, cells were stained with 5 μM CellTracker™ Green BODIPY™ Dye (Thermofisher, UK) for 30 min before imaging. Imaging was performed using a Nikon A1R confocal microscope with a Plan Apo VC 60x Oil, NA1.4, immersion objective. Green BODIPY™ Dye was excited at a wavelength of 522 nm and a 595/50 nm emission filter was applied, and a z-step size of 0.4 μm was used. Using ImageJ[46], the projection area of each cell was calculated from a manually-thresholded sum intensity projection of the entire z-stack. The contact area of each cell with the substrate was calculated similarly, but using only the 5 z-slices nearest to the material surface.

To image focal adhesions, cells were fixed for 10 min with 4% paraformaldehyde in phosphate-buffered saline (PBS), washed twice in PBS, and then permeabilized for 5 min with 0.1% Triton X-100 in PBS (PBS-T). After washing twice in PBS, cells were incubated for 1 h in 5% BSA in PBS-T at room temperature, and then with rabbit anti-Vinculin (Cell Signaling Technology #13901S) and mouse anti-α-tubulin antibodies (Sigma T5168), at 37°C in 5% BSA in PBS-T. After washing twice with PBS-T, cells were incubated for 1 h with fluorophore-conjugated anti-rabbit IgG Alexa Fluor®488 (Invitrogen A32731), anti-mouse IgG-Alexa Fluor®594 (Invitrogen, A-32744) and with Alexa Fluor®647 Phalloidin (to label actin; Cell Signaling Technology #8940S) at 37°C in 5% BSA in PBS-T. After washing twice with PBS-T, and once with milliQ H_2O, samples were mounted using ProLong™ Glass Antifade Mountant with NucBlue® (Invitrogen P36981). Images were captured on an upright Nikon A1+ confocal microscope with Plan Apo 60x Oil λS DIC N2, NA 1.4.

Measurement of cell mechanical properties using FluidFM: All experiments for cell elasticity/viscoelasticity and cell adhesion forces measurement were performed using the Flex FPM system (Nanosurf, Germany) which combines AFM and FluidFM technology (Cytosurge AG, Switzerland). The system was mounted on an Axio Observer Z1 inverted microscope (Carl Zeiss, Germany) fitted with 20x NA0.4 phase 2 DIC lens and a piezoelectric stage of 100 μm retraction range. The length and width of FluidFM cantilevers (Cytosurge AG, Switzerland) were 200 μm and 36 μm respectively, with spring constant of 2 N/m. In general, the choice of

cantilever spring constant may affect the determination of relaxation modulus based on finite element modelling and dimensional analysis [47]. A relatively large stiffness constant was chosen to accommodate the large adhesive force between cells and the material surface and to enable us to obtain the true equilibrium modulus [47]. The cantilever aperture was 8 μm (as shown in the scanning electron microscope image of the cantilever in Fig. S1 in the Supporting Information). Using the Cell Adhesion 100 μm workflow in Cytosurge software, approach-pause-grab operations were carried out for each cell. Fig.2 displays the typical schematic for the cell sucking process. The hollow cantilever approached cells until a setpoint of 200mV was reached (force equals 30-50 nN, depending on the different spring constants and deflection sensitivities of cantilevers used). The cantilever was held still for 2-3 seconds because we found that cantilever vibrations may occur after this time. Then a negative pressure of 800 mbar was applied to the micropipette using the pressure controller in the FluidFM probe to attach the cell to the cantilever, and the piezo stage-cantilever system was then used to retract the cantilever and pull the cell off the surface. Finally, a positive fluid pressure was applied through the cantilever to release the cell from the cantilever. Only isolated cells were measured to avoid cell-cell interactions.

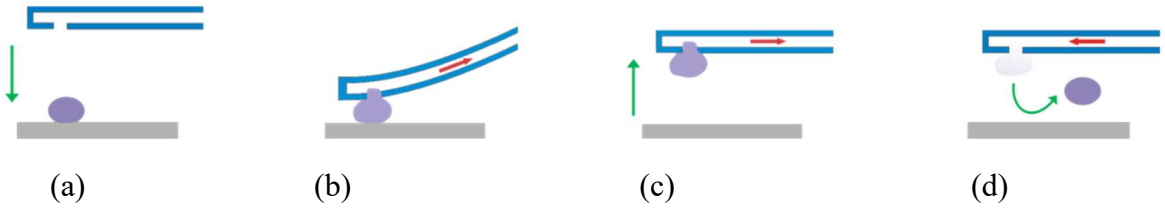

Figure 2. Schematic of cell sucking process using FluidFM. (a) Cantilever approaches the cell. (b) End of approach stage. The cantilever rests on the cell for 2-3 seconds, then negative pressure is applied via the microfluidics system. (c) The cell is moved away from the surface by Cantilever. (d) Positive fluid pressure releases the cell.

Cells were deformed when the probe reached the setpoint. In theory, the force-displacement curve during this approaching segment can be used to estimate the elastic modulus of the cell. However, the contact area and geometry between the cell and the cantilever was not constant during this period, which made it infeasible to calculate the elastic modulus of cell. During the 3 s pause, the cell exhibited stress relaxation (under keeping position mode). The stress relaxation was utilized to obtain a rough estimation of the viscoelastic properties because the cell contact area remained approximately constant as observed *in-situ* and could be estimated through the transparent cantilever (see Figure 3). Based on the detachment curve, the adhesive force could be easily determined. The adhesion work could also be determined by integration the force-displacement curve during the detachment test. A total of 95 measurements were performed.

Therefore, the force-displacement curves obtained during the whole process and the transparency of the cantilever enabled us to simultaneously measure both cell mechanics and cell-to-material adhesion.

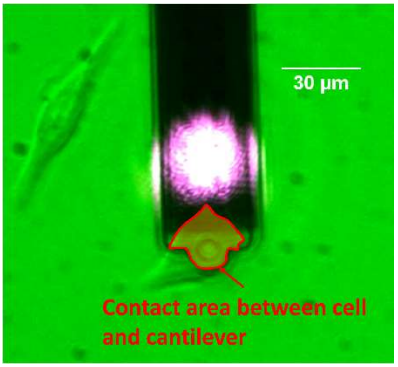

Figure 3. Representative image of the contact area between the cell and cantilever.

Analytical model

Contact areas between AFM probes and cells were estimated based on imaging through the transparent cantilever. The slight bending of cantilever had negligible effect on the contact area estimation, and we simplified the contact to a flat punch probe with complex geometry. Most studies have utilized only stress relaxation to obtain the viscoelastic properties of the cell by assuming step loading[48, 49]. However, the practical loading time is not infinitely small. Thus, we adopted the principle described by Chen and Lu[15] and used the following equation to analyse the stress relaxation curve.

$$F(t) = \frac{2R\delta}{1-\nu^2}\int_0^t E\left(t-t'\right)dt' \quad (1)$$

where F is the force, R is the equivalent radius of contact area, ν is Poisson's ratio, δ is the depth of indentation and *E(t)* is the relaxation modulus.

To describe the viscoelastic behavior of the living cell, the Prony series model was adopted. The normalized relaxation modulus given by the Prony series model is[50],

$$g(t) = g_\infty + \sum g_i exp\left(-\frac{t}{\tau_i}\right) \text{ , and } \quad g_\infty + \sum g_i = 1 \quad (2)$$

where g_∞ is the normalized equilibrium modulus, g_i is a material-related constant, and τ_i is the time constant.

The modulus and viscosity at each Maxwell arm can be determined by,

$$E_i = E_0 g_i \quad (3a)$$

$$\eta_i = E_i \tau_i \quad (3b)$$

Young's modulus, E, is given by

$$E = E_0 g_\infty \tag{3c}$$

where E_0 is the instantaneous elastic modulus.

These models have been demonstrated to describe well the time-dependent behaviour of different cells.[51-54]

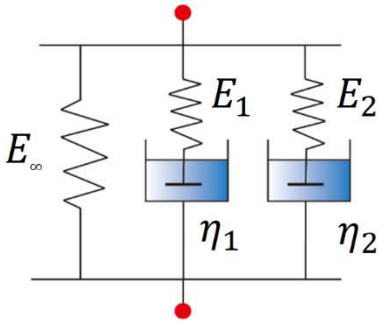

Figure 4. The schematic diagram of the Prony series model. Young's modulus $\boldsymbol{E}$ is also noted as equilibrium modulus $\boldsymbol{E}_\infty$.

If we assume i = 2 for the Prony series model (see Fig.4), we obtain the following equation

$$\begin{aligned} F(t) &= \frac{2R\delta}{1-v^2}\left[\int_0^{t_1} E\left(t-t'\right)dt' + \int_{t_1}^{t_2} E\left(t-t'\right)dt'\right] \\ &= \frac{2R\delta}{1-v^2}\int_0^{t_1}\left[E_0 - E_1\exp\left(-\frac{t-t'}{\tau_1}\right)\right. \\ &\quad \left. - E_2\exp\left(-\frac{t-t'}{\tau_2}\right)\right]dt' \end{aligned} \tag{4}$$

Solving this equation, we obtain,

$$F(t) = \frac{2R\delta}{1-v^2}E_0\left\{g_\infty + g_1\frac{\tau_1}{t_1}\exp\left(\frac{-t}{\tau_1}\right)\left[\exp\left(\frac{t_1}{\tau_1}\right)-1\right] + g_2\frac{\tau_2}{t_1}\exp\left(\frac{-t}{\tau_2}\right)\left[\exp\left(\frac{t_1}{\tau_2}\right)-1\right]\right\} \tag{5}$$

In this case, t_1 is the ramping time which is a constant for a given test. Living cells like MCF-7 are likely to be essentially incompressible materials[55], and we assumed $v = 0.5$. To avoid the issues caused by cantilever vibration at longer times (3-30s), curve fitting was done for the first 2-3 s of the stress relaxation curve. An in-house Matlab code was written to do curve fitting of the stress relaxation curve, which enabled us to determine $E_0, g_\infty, g_1, g_2, \tau_1, \tau_2$. Then, all the other physical parameters can be determined based on Equation (3). Our finite

element modelling has shown that use of this relative short relaxation period has a very small effect (<5%) on determining the time constants compared to longer stress relaxation times for the given cell properties in this study (data not shown). The adhesive force was directly determined from the detachment curve, and adhesion energy was determined by integrating force-displacement curves during detachment tests.

Statistical Analysis: Data were represented as mean values with standard error. Student's t-test was applied, where $p < 0.05$ was considered statistically significant. Pearson's test was used to examine if there was a correlation between the mechanical properties of the cells and cell-to-material adhesion. SPSS software (IBM®, USA) was used for statistical analyses.

RESULTS AND DISCUSSION

Cell shape is regulated by cell-to-material adhesion, which increases surface contact, and cortical tension, which reduces cell contacts. However, even cells of the same type on the same material often display different morphologies, mainly due to the heterogeneity of the cells or of the material surface[17, 56-58]. We wished to determine if cells with different morphologies exhibit different mechanics and adhesive strength.

MCF-7 cells plated on tissue culture treated polystyrene were observed to have different morphologies (e.g. round, spindle-like, and spread shapes, as shown in the video in the supporting information). We classified cells with different morphologies into two categories according to their thickness: thicker cells of above 10 μm (mainly of round or spindle-like shape), and flat cells below 10 μm (with well-spread disc-like shape). Immunofluorescence microscopy revealed that round and spindle-shaped cells had notably fewer detectable focal adhesions containing vinculin than well-spread flat cells (Figure 5a). We determined both the contact area between each cell and the surface (yellow areas in Fig 5b, c), and the total projection area for each cell (green in Fig. 5b, c) by analyzing confocal microscopic images as described in the Methods. The average projection area of thick cells was 430 ± 210 μm^2, while it was 740 ± 380 μm^2 for the thinner cells. The average contact areas of the two types were 230 ± 110 μm^2 and 680 ± 390 μm^2, respectively. There was significant difference in the projection area ($p = 0.028$) and the contact area ($p = 0.0015$) between the two categories of cell. The spreading ratios (the contact area over the projection area) of the thick and thinner cells were 0.55 ± 0.20 and 0.90 ± 0.07, respectively. The difference in spreading ratios was statistically significant ($p = 0.001$). In the following sections, thick cells are referred to as less-spread, and thinner cells as well-spread cells.

We then simultaneously determined the viscoelastic and adhesion properties of 29 less-spread and 18 well-spread MCF-7 cells using FluidFM. Fig. 6 displays representative force-

displacement curves of a less-spread cell and a well-spread cell during stress relaxation. The stress relaxation curves were fit well by equation (5) with $R > 0.99$ in all situations.

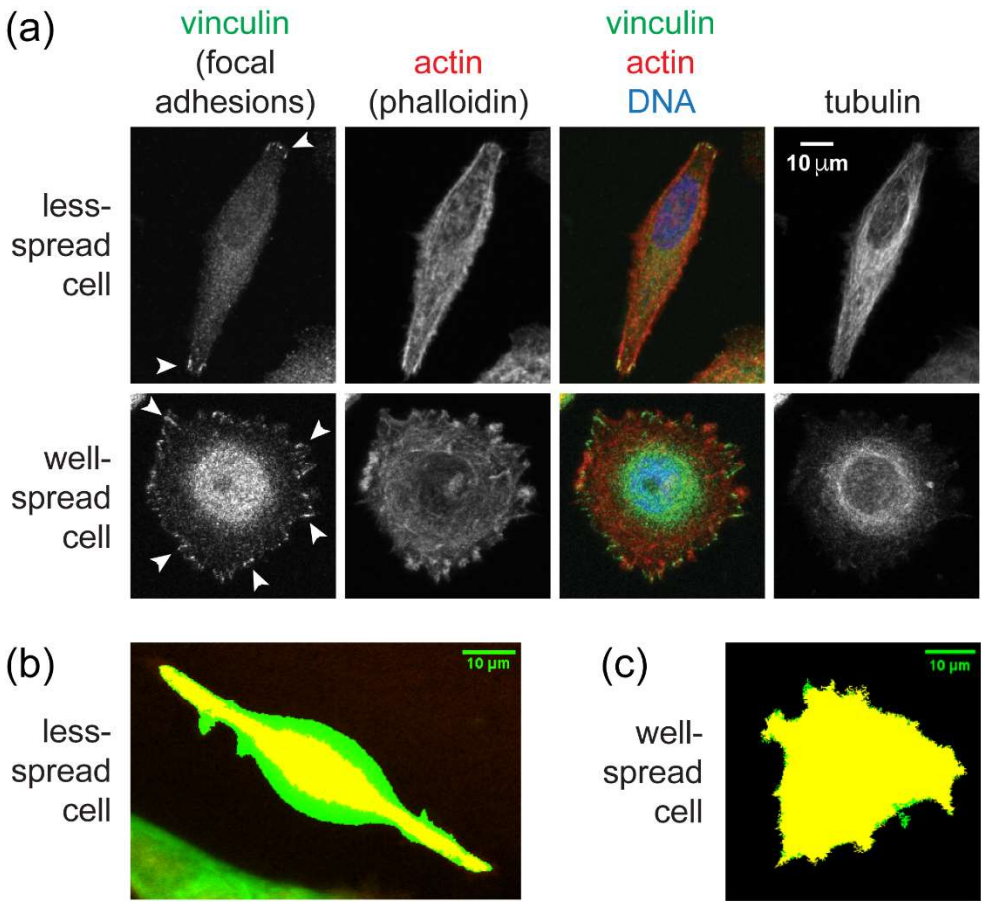

Figure 5. Representative confocal images of different MCF-7 cell morphologies. In (a), less-spread and well-spread cells were stained for vinculin to reveal focal adhesions (green; some examples are indicated with arrows), phalloidin to reveal actin (red), Hoechst 33342 to show DNA (blue) and for α-tubulin (grey). In (b), a thick less-spread cell and, in (c), a thinner well-spread cell were stained with CellTracker Green BODIPY™ dye to determine the projection area (green) and contact area (yellow).

Table 1 summarizes the key mechanical properties (e.g. viscoelastic properties, the adhesion force and adhesion work) of MCF-7 cells with different spreading ratios. The data analysis approach played a very important role here. If cells were assumed to be purely elastic, the mean apparent cell moduli of the same cell population seeded on the same surface were 0.56 kPa and 1.2 kPa for less-spread cells and well-spread cells, respectively. In other published work, the Young's moduli of MCF-7 cells were determined by fitting the loading curve with the Hertz model for a spherical probe[59]. However, cells exhibit viscoelastic characteristics and loading rates are not infinitely small. Therefore, the apparent value determined in this way can dramatically overestimate the Young's modulus[60]. In this paper, we only compare the elastic

moduli results to published studies which adopted appropriate viscoelastic models and considered the loading rate effect of the indenter.

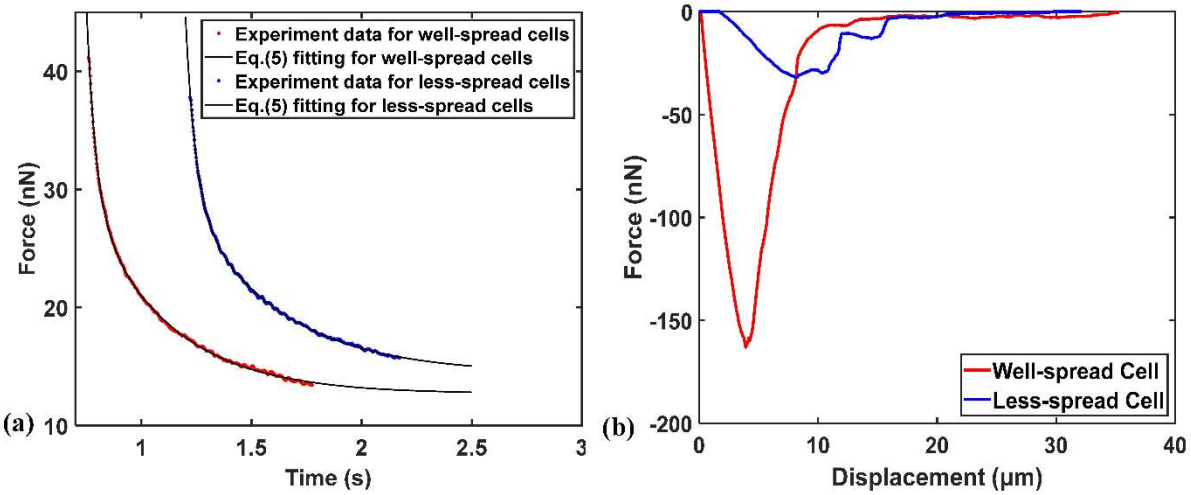

Figure 6. Representative curves for (a) stress relaxation when cantilever is resting on the cell at the end of approaching stage and (b) the subsequent detachment curves of a less-spread cell and well-spread cell.

We obtained equilibrium moduli and instantaneous moduli of approximately 0.2 kPa and 2 kPa, respectively. For well-spread cells, the thin layer effect could be significant at relatively large deformations when using pyramid or spherical indenters [24]. However, in our study, a flat punch indenter was used and the thin layer effect is not expected to be significant for the thickness/contact radius ratios and indentation depth/thickness ratio relevant here, consistent with computational modelling [61-63]. Therefore, a thin layer model similar to [24] was not considered.

Notably, these moduli were not significantly different between well-spread cells and less-spread cells ($p = 0.84$, 0.24 for equilibrium moduli and instantaneous moduli respectively). The Young's moduli determined here corresponded well to the reported values for MCF-7 cells determined using AFM methods and also taking the loading effect into account. For example, Young's (equilibrium) moduli of 0.2-0.5 kPa [64], and Young's moduli and instantaneous moduli of 0.26 ± 0.1 kPa and 1.2 ± 0.4 kPa respectively have been reported [60]. The results were also consistent with the Young's moduli (~0.4 kPa) of MCF-7 cells cultured on petri dishes for 1 day measured by optical tweezers [65], and with others utilizing oscillation induced deformation tests, where results between 0.2-0.3 kPa were obtained for MCF-7 cells with different morphologies[66].

The time constant τ_1 and τ_2 are important parameters to characterize the viscosity properties of cells (influenced mainly by the cytoplasm and actin networks[67, 68]), which reflect the

time that cells need to relax after a deformation. The difference between τ_1 for less-spread and well-spread cells was statistically significant (p = 0.00044), while there was no significant difference in τ_2 between less-spread and well-spread cells (p = 0.29). The maximum time constants (τ_2) determined here (approximately 0.6 s) were consistent with previously obtained values of 1 s which were based on curve fitting to creep tests using Kelvin-Viogt model[59]. η_1 and η_2 reflect the viscosity of cells and were defined previously. We have found that η_1 is higher for less-spread cells than well-spread cells, while that η_2 is higher for well-spread cells than less-spread cells. Other studies have demonstrated that $\boldsymbol{\eta_2}$ is often significantly higher than η_1 [50], as we found for well-spread cells. It has been suggested that these different viscosity components may be associated with viscosity of cytoplasm and cytoskeleton[67]. In our study, the overall viscosity (combination of η_1 and $\boldsymbol{\eta_2}$) was not significantly different for less-spread cells and well-spread cell (p = 0.06).

Table 1. Summary of key mechanical properties of MCF-7 cells with different spreading ratios.

	Less-spread cell (n=28)	Well-spread cell (n=19)	p value of difference
Instantaneous modulus $\boldsymbol{E_0}$ (kPa)	1.91± 0.71	2.12 ± 0.45	p = 0.24
Equilibrium modulus E_∞ (kPa)	0.21 ± 0.11	0.21 ± 0.10	p = 0.84
Time constant $\boldsymbol{\tau_1}$ (s)	0.10 ± 0.04	0.06 ± 0.02	p = 0.00044
Maxwell arm modulus E_1 (kPa)	1.56 ± 0.62	1.67 ± 0.47	p = 0.54
Viscosity coefficient $\boldsymbol{\eta_1}$ (Pa • s)	152 ± 88	103 ± 51	p = 0.023
Time constant $\boldsymbol{\tau_2}$ (s)	0.61 ± 0.27	0.55 ± 0.15	p = 0.29
Maxwell arm modulus E_2 (kPa)	0.13 ± 0.06	0.24 ± 0.076	p = 0.000004
Viscosity coefficient $\boldsymbol{\eta_2}$ (Pa • s)	81 ± 48	133 ± 50	p = 0.0025
Adhesive force F (nN)	50.2 ± 40.3	230 ± 295	p = 0.0028
Adhesion energy W (pJ)	0.37 ± 0.26	1.86± 2.89	p = 0.057
Max adhesion force displacement (μm)	11.45 ± 3.86	11.02 ± 7.16	p = 0.83
Fully detach displacement (μm)	22.14 ± 10.67	20.62 ± 7.96	p = 0.60

Cell viscosity is important as it can also be a mechanical biomarker for disease progression. For example, Alperen N *et al*. measured mouse ovarian surface epithelial cells using AFM, and found that the viscosity of the cells in the early stage of disease progression decreased significantly from 140 ± 100 Pa · s to 51 ± 30 Pa · s when reached the late stage of disease progression [69].

The measured adhesion force of MCF-7 cells on the petri dish is summarized in Table 1. Previously, it has been found that, for a given type of cell placed on different surfaces, the pulling distance required to detach a cell was longer on surfaces allowing stronger adhesive force. In this case, the work of adhesion was found to be proportional to the adhesive force. For example, when cell attached to the flat and pillars quartz surfaces, the average adhesion force of cells on the pillars surfaces was found to be half as the cells on flat surfaces, while the work of adhesion on former surface was about one third of the latter one[70].

Pearson's tests revealed a very strong correlation between the adhesion energy and adhesive force, (Pearson correlation = 0.976, Figure 7). There was no correlation between adhesion and the instantaneous modulus or equilibrium modulus. Also, the correlation between adhesion and viscosity was not statistically significant. However, there was a significant correlation between the adhesion force or energy and the viscous modulus (a function of the fitting parameter of g_1 and g_2 specified in equation (5); p = 0.006, 0.009 for adhesion force; p = 0.072, 0.039 for adhesion work). Although there were no significant differences in instantaneous or equilibrium moduli or time constants between less-spread and well-spread MCF-7 cells, the differences between the adhesion force (p = 0.0028) and the viscosity coefficients $\boldsymbol{\eta_1}$ and $\boldsymbol{\eta_2}$ were statistically significant (p = 0.023 and 0.0025).

When we plot the adhesion energy and adhesive force (see Fig. 7), the adhesion was proportional to the adhesive force for cells with both morphologies. This was consistent with the detachment distance values presented in Table 1, where the detachment distance for the less-spread and well-spread cells is almost the same. For the less-spread cells, the adhesive force and adhesion energy were weaker compared to their well-spread counterparts. As shown in Table 1, the adhesive force and work of adhesion for less-spread cells were about 5 times less than those for well spread cells. The contact areas of less-spread cells were 3 times lower than their well-spread counterparts. This correlation is most likely due to the lower number of cell receptors (e.g. integrins) engaged in contact between cell and substrate [59, 71, 72], consistent with the reduced numbers of focal adhesions we detected in less-spread cells (see Fig. 5). Indeed, the overall detachment force is the sum of the cohesive forces of the discrete cell receptor-to-surface bonds. In general, based on thermodynamics modelling, the abundance of integrin-ligand bonds is proportional to the total area of focal adhesions [73, 74], and focal adhesion area often correlates with the area of cell contact with the substrate[75]. Computational modelling also suggests stronger adhesion when focal adhesions are more abundant [76]. Therefore, higher cell contact area is likely to have higher adhesive force.

In the detachment curves, sometimes small force drops occurred before the whole cell detached from the surface (see Fig.S2), which were likely correlated to discrete detachment events prior to the whole cell detachment[34]. This may be associated with the contraction and detachment of membrane regions containing mature focal adhesions (see video S1 in Supporting Information). In general, these local detachment forces are on the order of 10 nN, similar to other cell detachment tests of mature adhesion states using FluidFM[34]. It should be noted that these forces are 2-3 orders of magnitude higher than those observed for rupture of the thin cell membrane tethers formed during short-term interactions between cells, or between cells and cantilevers [77, 78].

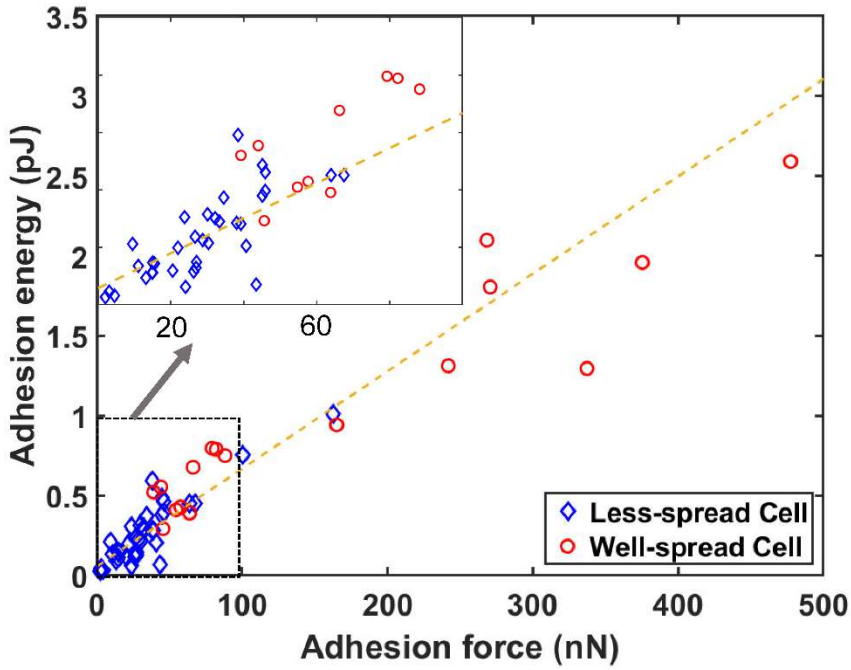

Figure 7. Plot of adhesion energy against adhesive force for less-spread cells and well-spread cells. In general, adhesion energy is proportional to adhesive force.

CONCLUSIONS

In summary, we report that simultaneous determination of both viscoelastic properties and adhesion of the same cell can be achieved with stress relaxation tests and subsequent pulling tests using fluidic force microscopy. The transparent cantilever enabled us to measure the contact area between cell and cantilever when determining the viscoelastic properties of cells. With appropriate mechanical models that consider the finite ramping time, we have found that MCF-7 cells on tissue-culture-treated polystyrene dishes have Young's moduli of about 0.2 kPa, regardless of their spreading ratios. The viscoelastic properties of MCF-7 cells determined here were consistent with AFM nanoindentation using spherical probes. Although the Young's modulus (equilibrium elastic modulus) and instantaneous elastic modulus were independent of

cell shape on the same surface, the viscosity of cells was slightly dependent on cell shape. The adhesive force was strongly dependent on the cell spreading ratio. This suggests that even fairly extensive differences in the morphology of cells and their cytoskeletons need not have a major effect their elastic properties if the cells are attached to the same surface. This experimental method and analytical approach could be a powerful tool for establishing quantitative correlations among different physical characteristics of numerous cell types in normal or diseased states, as well as elucidating the underpinning biological and pathological implications. This unique capacity of measuring viscoelastic properties and cell-materials adhesion of a single is important for the understanding of cell heterogeneity. We have also demonstrated that pulling tests using fluidic force microscopy can detect multiple discrete events that may be associated with the detachment of distinct focal adhesion-containing structures.

ASSOCIATED CONTENT

Supporting Information: Supporting Information is available free on the ACS Publications website at DOI: XXXXX. Fig. S1: Scanning electron microscope image of the cantilever. Fig S2: Images of representative changes on the detachment curves, which were captured before the whole cell was pulled away from the material surface. Video S1: The detachment process of a single cell using FluidFM.

AUTHOR INFORMATION

Corresponding Author

* *Jinju Chen: Email: jinju.chen@ncl.ac.uk*

Author Contributions

All authors contributed to this work. The study was conceived by J.C. J.C., M.L., J.M.G.H., WY designed the research. M.L. performed the majority of experiments and acquired the data. T.N.C. carried out immunofluorescence microscopy. M.L and J.C. did data analysis. J.C., J.M.G.H. and M.L. prepared the original draft. All authors reviewed and edited the manuscript. All authors have given approval to the final version of the manuscript.

ACKNOWLEDGMENTS

We also acknowledge technical support from Jack Dawson and Jake Sheriff and technicians in the mechanical engineering workshop, advice from Dr Mark Levasseur, and the help of Dr David Bulmer, Dr Emma Foster and Dr Alex Laude in the Newcastle University Bioimaging Facility. We also appreciate technical support from Dr. David Morgan and Dr. Henrik Peisker. J. Chen acknowledges funding from the Engineering and Physical Sciences Research Council (EP/R025606/1).

REFERENCES

[1] K. Dey, E. Roca, G. Ramorino, and L. Sartore, "Progress in the mechanical modulation of cell functions in tissue engineering," *Biomaterials Science,* vol. 8, no. 24, pp. 7033-7081, Dec 2020, doi: 10.1039/d0bm01255f.

[2] C. Kothapalli, G. Mahajan, and K. Farrell, "Substrate stiffness induced mechanotransduction regulates temporal evolution of human fetal neural progenitor cell phenotype, differentiation, and biomechanics," *Biomaterials Science,* vol. 8, no. 19, pp. 5452-5464, Oct 2020, doi: 10.1039/d0bm01349h.

[3] J. Chen *et al.*, "Cell Mechanics, Structure, and Function Are Regulated by the Stiffness of the Three-Dimensional Microenvironment," *Biophysical Journal,* vol. 103, no. 6, pp. 1188-1197, Sep 2012, doi: 10.1016/j.bpj.2012.07.054.

[4] A. Diz-Munoz, D. A. Fletcher, and O. D. Weiner, "Use the force: membrane tension as an organizer of cell shape and motility," *Trends in Cell Biology,* vol. 23, no. 2, pp. 47-53, Feb 2013, doi: 10.1016/j.tcb.2012.09.006.

[5] M. G. Haugh, C. M. Murphy, R. C. McKiernan, C. Altenbuchner, and F. J. O'Brien, "Crosslinking and Mechanical Properties Significantly Influence Cell Attachment, Proliferation, and Migration Within Collagen Glycosaminoglycan Scaffolds," *Tissue Engineering Part A,* vol. 17, no. 9-10, pp. 1201-1208, May 2011, doi: 10.1089/ten.tea.2010.0590.

[6] M. Lekka, P. Laidler, D. Gil, J. Lekki, Z. Stachura, and A. Z. Hrynkiewicz, "Elasticity of normal and cancerous human bladder cells studied by scanning force microscopy," *European Biophysics Journal with Biophysics Letters,* vol. 28, no. 4, pp. 312-316, 1999, doi: 10.1007/s002490050213.

[7] D. Dutta, X. L. Palmer, J. Ortega-Rodas, V. Balraj, I. G. Dastider, and S. Chandra, "Biomechanical and Biophysical Properties of Breast Cancer Cells Under Varying Glycemic Regimens," *Breast Cancer-Basic and Clinical Research,* vol. 14, Nov 2020, Art no. 1178223420972362, doi: 10.1177/1178223420972362.

[8] M. Lekka, "Discrimination Between Normal and Cancerous Cells Using AFM," *Bionanoscience,* vol. 6, no. 1, pp. 65-80, Mar 2016, doi: 10.1007/s12668-016-0191-3.

[9] Q. S. Li, G. Y. H. Lee, C. N. Ong, and C. T. Lim, "AFM indentation study of breast cancer cells," *Biochemical and Biophysical Research Communications,* vol. 374, no. 4, pp. 609-613, Oct 2008, doi: 10.1016/j.bbrc.2008.07.078.

[10] D. Ghosh and M. R. Dawson, "Microenvironment Influences Cancer Cell Mechanics from Tumor Growth to Metastasis," in *Biomechanics in*

Oncology, vol. 1092, C. Dong, N. Zahir, and K. Konstantopoulos Eds., (Advances in Experimental Medicine and Biology, 2018, pp. 69-90.

[11] S. Azadi, M. Tafazzoli-Shadpour, M. Soleimani, and M. E. Warkiani, "Modulating cancer cell mechanics and actin cytoskeleton structure by chemical and mechanical stimulations," *Journal of Biomedical Materials Research Part A,* vol. 107, no. 8, pp. 1569-1581, Aug 2019, doi: 10.1002/jbm.a.36670.

[12] S. Suresh, "Biomechanics and biophysics of cancer cells," *Acta Biomaterialia,* vol. 3, no. 4, pp. 413-438, Jul 2007, doi: 10.1016/j.actbio.2007.04.002.

[13] M. Janiszewska, M. C. Primi, and T. Izard, "Cell adhesion in cancer: Beyond the migration of single cells," *Journal of Biological Chemistry,* vol. 295, no. 8, pp. 2495-2505, Feb 2020, doi: 10.1074/jbc.REV119.007759.

[14] J. J. Chen, "Nanobiomechanics of living cells: a review," *Interface Focus,* vol. 4, no. 2, Apr 2014, Art no. 20130055, doi: 10.1098/rsfs.2013.0055.

[15] J. J. Chen and G. X. Lu, "Finite element modelling of nanoindentation based methods for mechanical properties of cells," *Journal of Biomechanics,* vol. 45, no. 16, pp. 2810-2816, Nov 2012, doi: 10.1016/j.jbiomech.2012.08.037.

[16] G. T. Charras and M. A. Horton, "Single cell mechanotransduction and its modulation analyzed by atomic force microscope indentation," *Biophysical Journal,* vol. 82, no. 6, pp. 2970-2981, Jun 2002, doi: 10.1016/s0006-3495(02)75638-5.

[17] S. Barreto, C. H. Clausen, C. M. Perrault, D. A. Fletcher, and D. Lacroix, "A multi-structural single cell model of force-induced interactions of cytoskeletal components," *Biomaterials,* vol. 34, no. 26, pp. 6119-6126, Aug 2013, doi: 10.1016/j.biomaterials.2013.04.022.

[18] C. R. Guerrero, P. D. Garcia, and R. Garcia, "Subsurface Imaging of Cell Organelles by Force Microscopy," *Acs Nano,* vol. 13, no. 8, pp. 9629-9637, Aug 2019, doi: 10.1021/acsnano.9b04808.

[19] G. T. Charras and M. A. Horton, "Determination of cellular strains by combined atomic force microscopy and finite element modeling," *Biophysical Journal,* vol. 83, no. 2, pp. 858-879, Aug 2002, doi: 10.1016/s0006-3495(02)75214-4.

[20] P. Carl and H. Schillers, "Elasticity measurement of living cells with an atomic force microscope: data acquisition and processing," *Pflugers Archiv-European Journal of Physiology,* vol. 457, no. 2, pp. 551-559, Nov 2008, doi: 10.1007/s00424-008-0524-3.

[21] W. J. Yang, D. Lacroix, L. P. Tan, and J. J. Chen, "Revealing the nanoindentation response of a single cell using a 3D structural finite element model," *Journal of Materials Research,* vol. in press, pp.

DOI:10.1557/s43578-020-00004-5, 2021, doi: 10.1557/s43578-020-00004-5.

[22] J. A. C. Santos, L. M. Rebelo, A. C. Araujo, E. B. Barros, and J. S. de Sousa, "Thickness-corrected model for nanoindentation of thin films with conical indenters," *Soft Matter,* vol. 8, no. 16, pp. 4441-4448, 2012, doi: 10.1039/c2sm07062f.

[23] E. M. Darling, S. Zauscher, J. A. Block, and F. Guilak, "A thin-layer model for viscoelastic, stress-relaxation testing of cells using atomic force microscopy: Do cell properties reflect metastatic potential?," *Biophysical Journal,* vol. 92, no. 5, pp. 1784-1791, Mar 2007, doi: 10.1529/biophysj.106.083097.

[24] E. K. Dimitriadis, F. Horkay, J. Maresca, B. Kachar, and R. S. Chadwick, "Determination of elastic moduli of thin layers of soft material using the atomic force microscope," *Biophysical Journal,* vol. 82, no. 5, pp. 2798-2810, May 2002, doi: 10.1016/s0006-3495(02)75620-8.

[25] W. R. Bowen, N. Hilal, R. W. Lovitt, and C. J. Wright, "Direct measurement of the force of adhesion of a single biological cell using an atomic force microscope," *Colloids and Surfaces a-Physicochemical and Engineering Aspects,* vol. 136, no. 1-2, pp. 231-234, Apr 1998, doi: 10.1016/s0927-7757(97)00243-4.

[26] J. Friedrichs *et al.*, "A practical guide to quantify cell adhesion using single-cell force spectroscopy," *Methods,* vol. 60, no. 2, pp. 169-178, Apr 2013, doi: 10.1016/j.ymeth.2013.01.006.

[27] J. L. Maciaszek, K. Partola, J. Zhang, B. Andemariam, and G. Lykotrafitis, "Single-cell force spectroscopy as a technique to quantify human red blood cell adhesion to subendothelial laminin," *Journal of Biomechanics,* vol. 47, no. 16, pp. 3855-3861, Dec 2014, doi: 10.1016/j.jbiomech.2014.10.016.

[28] G. Weder *et al.*, "The quantification of single cell adhesion on functionalized surfaces for cell sheet engineering," *Biomaterials,* vol. 31, no. 25, pp. 6436-6443, Sep 2010, doi: 10.1016/j.biomaterials.2010.04.068.

[29] P. Dorig *et al.*, "Force-controlled spatial manipulation of viable mammalian cells and micro-organisms by means of FluidFM technology," *Applied Physics Letters,* vol. 97, no. 2, Jul 2010, Art no. 023701, doi: 10.1063/1.3462979.

[30] O. Guillaume-Gentil, E. Potthoff, D. Ossola, C. M. Franz, T. Zambelli, and J. A. Vorholt, "Force-controlled manipulation of single cells: from AFM to FluidFM," *Trends in Biotechnology,* vol. 32, no. 7, pp. 381-388, Jul 2014, doi: 10.1016/j.tibtech.2014.04.008.

[31] M. Y. Amarouch, J. El Hilaly, and D. Mazouzi, "AFM and FluidFM Technologies: Recent Applications in Molecular and Cellular Biology," *Scanning,* 2018, Art no. 7801274, doi: 10.1155/2018/7801274.

[32] P. Saha, T. Duanis-Assaf, and M. Reches, "Fundamentals and Applications of FluidFM Technology in Single-Cell Studies," *Advanced Materials*

Interfaces, vol. 7, no. 23, Dec 2020, Art no. 2001115, doi: 10.1002/admi.202001115.
[33] M. K. Ghatkesar, H. H. P. Garza, and U. Staufer, "Hollow AFM cantilever pipette," *Microelectronic Engineering,* vol. 124, pp. 22-25, Jul 2014, doi: 10.1016/j.mee.2014.04.019.
[34] P. Wysotzki, A. Sancho, J. Gimsa, and J. Groll, "A comparative analysis of detachment forces and energies in initial and mature cell-material interaction," *Colloids and Surfaces B-Biointerfaces,* vol. 190, Jun 2020, Art no. 110894, doi: 10.1016/j.colsurfb.2020.110894.
[35] D. E. Ingber, "Tensegrity I. Cell structure and hierarchical systems biology," (in eng), *J Cell Sci,* vol. 116, no. Pt 7, pp. 1157-73, Apr 1 2003, doi: 10.1242/jcs.00359.
[36] D. E. Ingber, "Tensegrity II. How structural networks influence cellular information processing networks," *Journal of cell science,* vol. 116, no. 8, pp. 1397-1408, 2003.
[37] L. Jaatinen, E. Young, J. Hyttinen, J. Vörös, T. Zambelli, and L. Demkó, "Quantifying the effect of electric current on cell adhesion studied by single-cell force spectroscopy," *Biointerphases,* vol. 11, no. 1, p. 011004, 2016.
[38] J. Chen and S. Bull, "Finite element analysis of contact induced adhesion failure in multilayer coatings with weak interfaces," *Thin Solid Films,* vol. 517, no. 13, pp. 3704-3711, 2009.
[39] J. Ferlay *et al.*, "Cancer incidence and mortality worldwide: Sources, methods and major patterns in GLOBOCAN 2012," *International Journal of Cancer,* vol. 136, no. 5, pp. E359-E386, Mar 2015, doi: 10.1002/ijc.29210.
[40] H. A. Moayyer, M. Naderi, and J. A. Mohandesi, "Synthesis and Nanomechanical Properties of Polystyrene/Silica Core/Shell Particles Via Atomic Force Microscopy," *Langmuir,* vol. 37, no. 35, pp. 10602-10611, Sep 2021, doi: 10.1021/acs.langmuir.1c01918.
[41] J. Li, F. Zhang, L. L. Jiang, L. Yu, and L. X. Zhang, "Preparation of Silica@Silica Core-Shell Microspheres Using an Aqueous Two-Phase System in a Novel Microchannel Device," *Langmuir,* vol. 36, no. 2, pp. 576-584, Jan 2020, doi: 10.1021/acs.langmuir.9b03034.
[42] Y. Nakamura, Y. Iso, and T. Isobe, "Bandgap-Tuned CuInS2/ZnS Core/Shell Quantum Dots for a Luminescent Downshifting Layer in a Crystalline Silicon Solar Module," *Acs Applied Nano Materials,* vol. 3, no. 4, pp. 3417-3426, Apr 2020, doi: 10.1021/acsanm.0c00175.
[43] M. Schroffenegger *et al.*, "Polymer Topology Determines the Formation of Protein Corona on Core-Shell Nanoparticles," *Acs Nano,* vol. 14, no. 10, pp. 12708-12718, Oct 2020, doi: 10.1021/acsnano.0c02358.
[44] J. Park and P. S. Doyle, "Multifunctional Hierarchically-Assembled Hydrogel Particles with Pollen Grains via Pickering Suspension

Polymerization," *Langmuir,* vol. 34, no. 48, pp. 14643-14651, Dec 2018, doi: 10.1021/acs.langmuir.8b02957.

[45] Y. L. Lai, H. Zhang, Y. Sugano, H. Xie, and P. Kallio, "Correlation of Surface Morphology and Interfacial Adhesive Behavior between Cellulose Surfaces: Quantitative Measurements in Peak-Force Mode with the Colloidal Probe Technique," *Langmuir,* vol. 35, no. 22, pp. 7312-7321, Jun 2019, doi: 10.1021/acs.langmuir.8b03503.

[46] J. Schindelin *et al.*, "Fiji: an open-source platform for biological-image analysis," *Nature Methods,* vol. 9, no. 7, pp. 676-682, 2012/07/01 2012, doi: 10.1038/nmeth.2019.

[47] J. Y. Sheng, C. Mo, G. Y. Li, H. C. Zhao, Y. P. Cao, and X. Q. Feng, "AFM-based indentation method for measuring the relaxation property of living cells," *Journal of Biomechanics,* vol. 122, Jun 2021, Art no. 110444, doi: 10.1016/j.jbiomech.2021.110444.

[48] E. M. Darling, S. Zauscher, and F. Guilak, "Viscoelastic properties of zonal articular chondrocytes measured by atomic force microscopy," *Osteoarthritis and Cartilage,* vol. 14, no. 6, pp. 571-579, Jun 2006, doi: 10.1016/j.joca.2005.12.003.

[49] E. M. Darling, M. Topel, S. Zauscher, T. P. Vail, and F. Guilak, "Viscoelastic properties of human mesenchymally-derived stem cells and primary osteoblasts, chondrocytes, and adipocytes," *Journal of Biomechanics,* vol. 41, no. 2, pp. 454-464, 2008, doi: 10.1016/j.jbiomech.2007.06.019.

[50] S. Moreno-Flores, R. Benitez, M. D. Vivanco, and J. L. Toca-Herrera, "Stress relaxation and creep on living cells with the atomic force microscope: a means to calculate elastic moduli and viscosities of cell components," *Nanotechnology,* vol. 21, no. 44, Nov 2010, Art no. 445101, doi: 10.1088/0957-4484/21/44/445101.

[51] W. R. Trickey, G. M. Lee, and F. Guilak, "Viscoelastic properties of chondrocytes from normal and osteoarthritic human cartilage," *Journal of Orthopaedic Research,* vol. 18, no. 6, pp. 891-898, Nov 2000, doi: 10.1002/jor.1100180607.

[52] W. R. Trickey, T. P. Vail, and F. Guilak, "The role of the cytoskeleton in the viscoelastic properties of human articular chondrocytes," *Journal of Orthopaedic Research,* vol. 22, no. 1, pp. 131-139, Jan 2004, doi: 10.1016/s0736-0266(03)00150-5.

[53] W. P. Duan *et al.*, "Normal age-related viscoelastic properties of chondrons and chondrocytes isolated from rabbit knee," *Chinese Medical Journal,* vol. 125, no. 14, pp. 2574-2581, Jul 2012, doi: 10.3760/cma.j.issn.0366-6999.2012.14.032.

[54] J. Chen, D. L. Bader, D. A. Lee, and M. M. Knight, "Finite element modeling of cell deformation when chondrocyte seeded agarose is subjected to compression.," *Proceedings of the 8th International*

Conference on Cell and Stem Cell Engineering (ICCE) IFMBE Proceedings, vol. 30, pp. 17–20, 2011.

[55] N. Nijenhuis, X. Zhao, A. Carisey, C. Ballestrem, and B. Derby, "Combining AFM and Acoustic Probes to Reveal Changes in the Elastic Stiffness Tensor of Living Cells," *Biophysical Journal,* vol. 107, no. 7, pp. 1502-1512, 2014/10/07/ 2014, doi: 10.1016/j.bpj.2014.07.073.

[56] P. F. Duan *et al.*, "How cell culture conditions affect the microstructure and nanomechanical properties of extracellular matrix formed by immortalized human mesenchymal stem cells: An experimental and modelling study," *Materials Science & Engineering C-Materials for Biological Applications,* vol. 89, pp. 149-159, Aug 2018, doi: 10.1016/j.msec.2018.03.027.

[57] E. Grigoriou, M. Cantini, M. J. Dalby, A. Petersen, and M. Salmeron-Sanchez, "Cell migration on material-driven fibronectin microenvironments," *Biomaterials Science,* vol. 5, no. 7, pp. 1326-1333, Jul 2017, doi: 10.1039/c7bm00333a.

[58] N. Gavara and R. Chadwick, "Relationship between cell stiffness and stress fiber amount, assessed by simultaneous atomic force microscopy and live-cell fluorescence imaging," *Biomechanics and Modeling in Mechanobiology,* vol. 15, no. 3, pp. 511-523, Jun 2016, doi: 10.1007/s10237-015-0706-9.

[59] M. H. Korayem, Y. H. Sooha, and Z. Rastegar, "MCF-7 cancer cell apparent properties and viscoelastic characteristics measurement using AFM," *Journal of the Brazilian Society of Mechanical Sciences and Engineering,* vol. 40, no. 6, Jun 2018, Art no. 297, doi: 10.1007/s40430-018-1214-5.

[60] Y. M. Efremov, W. H. Wang, S. D. Hardy, R. L. Geahlen, and A. Raman, "Measuring nanoscale viscoelastic parameters of cells directly from AFM force-displacement curves," *Scientific Reports,* vol. 7, May 2017, Art no. 1541, doi: 10.1038/s41598-017-01784-3.

[61] A. S. Vasiliev, S. S. Volkov, S. M. Aizikovich, and B. I. Mitrin, "Plane contact problem on indentation of a flat punch into a transversely-isotropic half-plane with functionally graded transversely-isotropic coating," *Zeitschrift Fur Angewandte Mathematik Und Physik,* vol. 68, no. 1, Feb 2017, Art no. 4, doi: 10.1007/s00033-016-0746-8.

[62] Y. P. Cao, D. C. Ma, and D. Raabe, "The use of flat punch indentation to determine the viscoelastic properties in the time and frequency domains of a soft layer bonded to a rigid substrate," *Acta Biomaterialia,* vol. 5, no. 1, pp. 240-248, Jan 2009, doi: 10.1016/j.actbio.2008.07.020.

[63] O. Brazil *et al.*, "In situ measurement of bulk modulus and yield response of glassy thin films via confined layer compression," *Journal of Materials Research,* vol. 35, no. 6, pp. 644-653, Mar 2020, doi: 10.1557/jmr.2020.42.

[64] F.-S. Quan and K. S. Kim, "Medical applications of the intrinsic mechanical properties of single cells," *Acta Biochimica et Biophysica Sinica,* vol. 48, no. 10, pp. 865-871, 2016, doi: 10.1093/abbs/gmw081.
[65] T. Fischer, A. Hayn, and C. T. Mierke, "Effect of Nuclear Stiffness on Cell Mechanics and Migration of Human Breast Cancer Cells," *Frontiers in Cell and Developmental Biology,* vol. 8, May 2020, Art no. 393, doi: 10.3389/fcell.2020.00393.
[66] O. O. Adeniba, E. A. Corbin, A. Ganguli, Y. Kim, and R. Bashir, "Simultaneous time-varying viscosity, elasticity, and mass measurements of single adherent cancer cells across cell cycle," *Scientific Reports,* vol. 10, no. 1, Jul 2020, Art no. 12803, doi: 10.1038/s41598-020-69638-z.
[67] J. Schnauß *et al.*, "Cells in Slow Motion: Apparent Undercooling Increases Glassy Behavior at Physiological Temperatures," *Advanced Materials,* p. 2101840, 2021.
[68] M. Li, L. Liu, X. Xiao, N. Xi, and Y. Wang, "Effects of methotrexate on the viscoelastic properties of single cells probed by atomic force microscopy," *Journal of biological physics,* vol. 42, no. 4, pp. 551-569, 2016.
[69] A. N. Ketene, E. M. Schmelz, P. C. Roberts, and M. Agah, "The effects of cancer progression on the viscoelasticity of ovarian cell cytoskeleton structures," *Nanomedicine: Nanotechnology, Biology and Medicine,* vol. 8, no. 1, pp. 93-102, 2012/01/01/ 2012, doi: https://doi.org/10.1016/j.nano.2011.05.012.
[70] G. Weder *et al.*, "Use of Force Spectroscopy to Investigate the Adhesion of Living Adherent Cells," *Langmuir,* vol. 26, no. 11, pp. 8180-8186, Jun 2010, doi: 10.1021/la904526u.
[71] J. Iturri *et al.*, "Resveratrol-Induced Temporal Variation in the Mechanical Properties of MCF-7 Breast Cancer Cells Investigated by Atomic Force Microscopy," *International Journal of Molecular Sciences,* vol. 20, no. 13, Jul 2019, Art no. 3275, doi: 10.3390/ijms20133275.
[72] M. H. Korayem and Z. Rastegar, "Experimental Characterization of MCF-10A Normal Cells Using AFM: Comparison with MCF-7 Cancer Cells," *Molecular & Cellular Biomechanics,* vol. 16, no. 2, p. 109, 2019.
[73] E. McEvoy, V. S. Deshpande, and P. McGarry, "Free energy analysis of cell spreading," *Journal of the Mechanical Behavior of Biomedical Materials,* vol. 74, pp. 283-295, Oct 2017, doi: 10.1016/j.jmbbm.2017.06.006.
[74] E. McEvoy, S. S. Shishvan, V. S. Deshpande, and J. P. McGarry, "Thermodynamic Modeling of the Statistics of Cell Spreading on Ligand-Coated Elastic Substrates," *Biophysical Journal,* vol. 115, no. 12, pp. 2451-2460, Dec 2018, doi: 10.1016/j.bpj.2018.11.007.
[75] C. F. Natale, J. Lafaurie-Janvore, M. Ventre, A. Babataheri, and A. I. Barakat, "Focal adhesion clustering drives endothelial cell morphology on

patterned surfaces," *Journal of the Royal Society Interface,* vol. 16, no. 158, Sep 2019, Art no. 20190263, doi: 10.1098/rsif.2019.0263.
[76] J. P. McGarry *et al.*, "Simulation of the contractile response of cells on an array of micro-posts," *Philosophical Transactions of the Royal Society a-Mathematical Physical and Engineering Sciences,* vol. 367, no. 1902, pp. 3477-3497, Sep 2009, doi: 10.1098/rsta.2009.0097.
[77] M. Z. Sun *et al.*, "Multiple membrane tethers probed by atomic force microscopy," *Biophysical Journal,* vol. 89, no. 6, pp. 4320-4329, Dec 2005, doi: 10.1529/biophysj.104.058180.
[78] P. H. Puech, K. Poole, D. Knebel, and D. J. Muller, "A new technical approach to quantify cell-cell adhesion forces by AFM," *Ultramicroscopy,* vol. 106, no. 8-9, pp. 637-644, Jun-Jul 2006, doi: 10.1016/j.ultramic.2005.08.003.

For Table of Contents Use Only

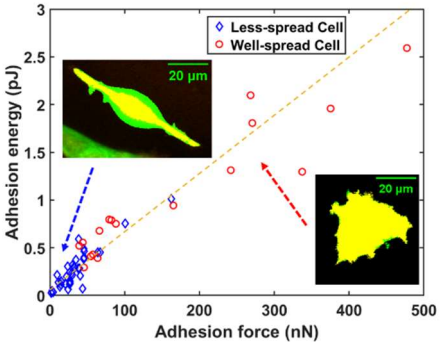

Supporting Information

Simultaneous measurement of single cell mechanics and cell-to-materials adhesion using fluidic force microscopy

Ma Luo[†], Wenjian Yang[†,#], Tyrell N. Cartwright[‡], Jonathan M.G. Higgins[‡], and Jinju Chen[†]*

[†] School of Engineering, Newcastle University, Newcastle Upon Tyne, NE1 7RU, UK; [#] Research Center for Intelligent Sensing Systems, Zhijiang Laboratory, Hangzhou, 311100, China; [‡]Biosciences Institute, Faculty of Medical Sciences, Newcastle University, Framlington Place, Newcastle upon Tyne, NE2 4HH, UK.

* Correspondence and requests for materials should be addressed to J.C. (email: jinju.chen@ncl.ac.uk)

Number of Pages: 2

Number of Figures: 2

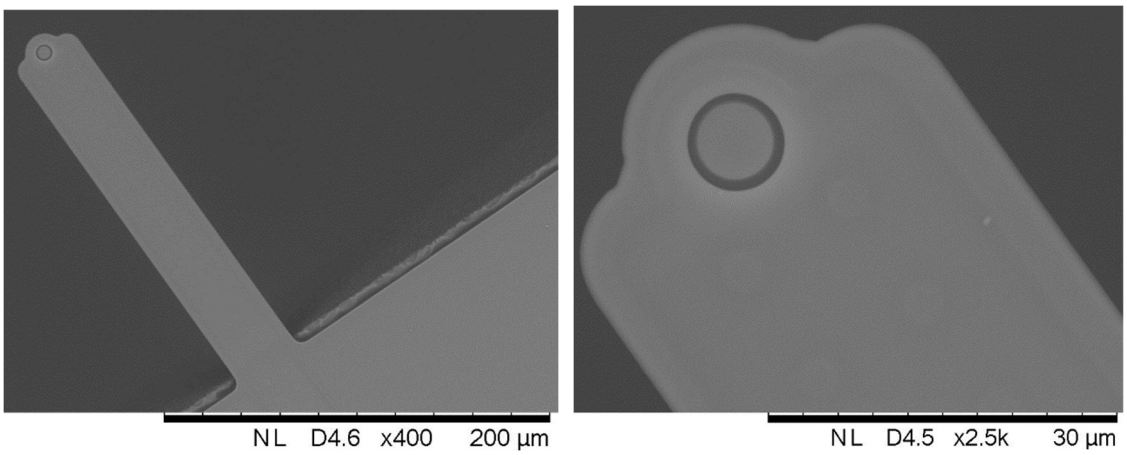

Figure S1: The scanning electron microscope image of the cantilever for FluidFM used in this study .

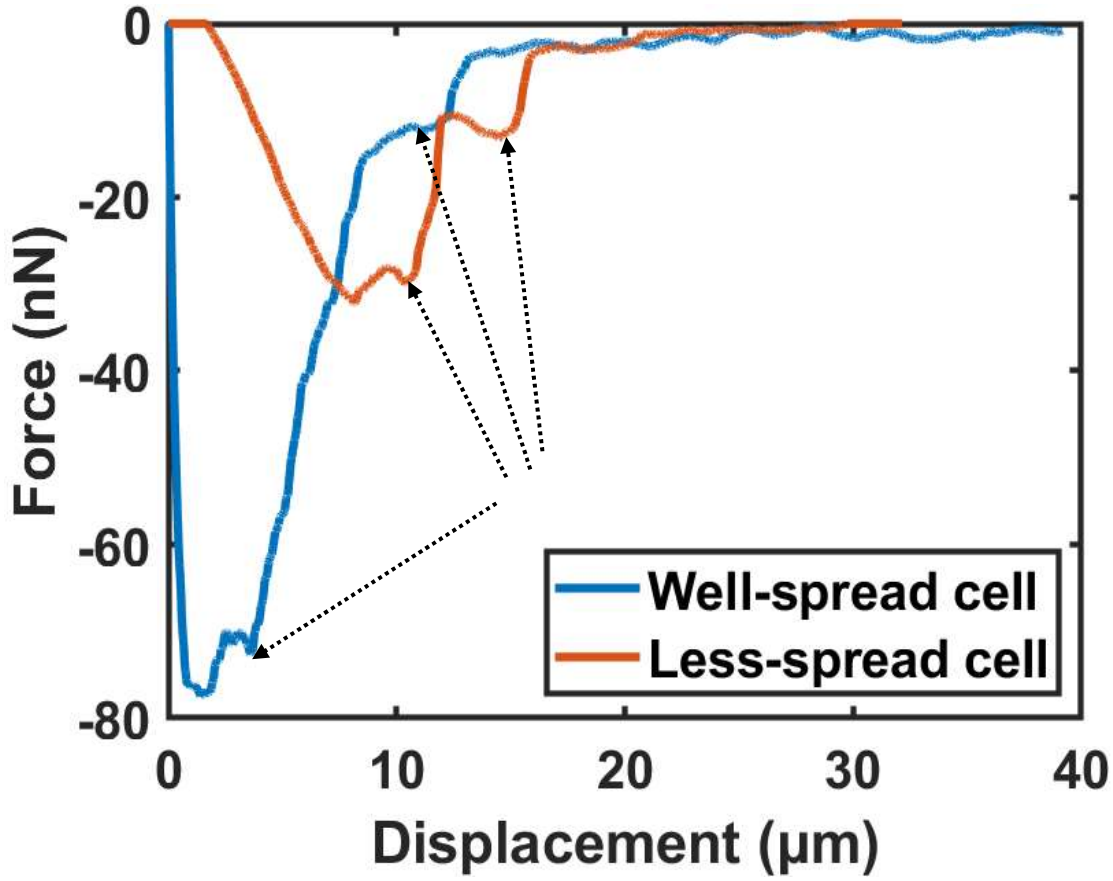

Figure S2: Representative images of multiple events on the detachment curves for both less-spread cell and well-spread cell, which can be related to detachment of distinct focal adhesion-containing structures.